VHF signal power suppression in stratiform and convective precipitation

A. J. Mcdonald, K. P. Monahan, D. A. Hooper, C. Gaffard

Annales Geophysicae, 24, 23–35, 2006
SRef-ID: 1432-0576/ag/2006-24-23

Annales Geophysicae

VHF signal power suppression in stratiform and convective precipitation

A. J. McDonald[1], **K. P. Monahan**[1], **D. A. Hooper**[2], **and C. Gaffard**[3]

[1]Department of Physics and Astronomy, University of Canterbury, Christchurch, New Zealand
[2]Rutherford Appleton Laboratory, Chilton, Didcot, Oxon, OX11 0QX, UK
[3]Met Office, University of Reading, Meteorology Building, PO Box 243, Earley Gate, Reading, RG6 6BB, UK

Received: 24 February 2005 – Revised: 30 November 2005 – Accepted: 1 December 2005 – Published: 7 March 2006

Abstract. Previous studies have indicated that VHF clear-air radar return strengths are reduced during periods of precipitation. This study aims to examine whether the type of precipitation, stratiform and convective precipitation types are identified, has any impact on the relationships previously observed and to examine the possible mechanisms which produce this phenomenon. This study uses a combination of UHF and VHF wind-profiler data to define periods associated with stratiform and convective precipitation. This identification is achieved using an algorithm which examines the range squared corrected signal to noise ratio of the UHF returns for a bright band signature for stratiform precipitation. Regions associated with convective rainfall have been defined by identifying regions of enhanced range corrected signal to noise ratio that do not display a bright band structure and that are relatively uniform until a region above the melting layer.

This study uses a total of 68 days, which incorporated significant periods of surface rainfall, between 31 August 2000 and 28 February 2002 inclusive from Aberystwyth (52.4° N, 4.1° W). Examination suggests that both precipitation types produce similar magnitude reductions in VHF signal power on average. However, the frequency of occurrence of statistically significant reductions in VHF signal power are very different. In the altitude range 2–4 km stratiform precipitation is related to VHF signal suppression approximately 50% of the time while in convective precipitation suppression is observed only 27% of the time. This statistical result suggests that evaporation, which occurs more often in stratiform precipitation, is important in reducing the small-scale irregularities in humidity and thereby the radio refractive index. A detailed case study presented also suggests that evaporation reducing small-scale irregularities in humidity may contribute to the observed VHF signal suppression.

Keywords. Meteorology and atmospheric dynamics (Precipitation) – Radio science (Remote sensing; Instruments and techniques)

Correspondence to: A. J. McDonald
(adrian.mcdonald@canterbury.ac.nz)

1 Introduction

Wind profiler radars operating at very high and ultra high frequencies (VHF and UHF, respectively) are sensitive to both clear air returns, from radio refractive index irregularities, and Rayleigh scattering, from hydrometeors. The dependence of both mechanisms on wavelength means that UHF and VHF radars have very different sensitivities to these processes. Ralph (1995) indicates that only under conditions of heavy rainfall is the Rayleigh scattered signal expected to be larger than the clear-air return for VHF wind-profilers. Whereas light rain or drizzle is all that is necessary for the return from hydrometeors to be larger than that from the clear-air for UHF wind-profilers. While this is true in general, several studies (Chu and Lin, 1994; Cohn et al., 1995; Vaughan and Worthington, 2000; McDonald et al., 2004) have suggested that processes associated with precipitation can directly impact the magnitude of the clear-air signal. Chu and Lin (1994) indicated that heavy convective precipitation suppresses VHF radar clear-air returns which they attributed to the effect of entrainment of dry, cold air into a warm, moist cloud. The relationship between temperature and humidity fluctuations associated with this process would act to reduce the magnitude of refractive index irregularities, to which the radar reflectivity is directly related. This possibility is supported by Rao et al. (1999) which indicated that the weakening of the clear air echo observed at the bright band in stratiform precipitation might also be due to the turbulent mixing between warm and humid in-cloud air and colder and drier surrounding air. Alternatively, Vaughan and Worthington (2000) proposes that the reduction in VHF signal power returned is produced by heavy precipitation acting as a source of moisture which tends to "wash out" small-scale irregularities in humidity, bringing the air to the local saturated vapour pressure. The work of Vaughan and Worthington (2000) suggests that this mechanism is not specific to periods associated with convective rainfall as previously suggested by Chu and Lin (1994) and Chu and Song (1998). Indeed, Houze (1997) implies that evaporation is more often observed in stratiform precipitation. Work by McDonald et al. (2004)

also suggests that the VHF clear-air signal is suppressed during precipitation. Their study indicates that there may be a difference between the magnitude of the suppression associated with different precipitation types. This study aims to determine whether different types of rainfall, separated into stratiform and convective types, have different effects on the magnitude of the VHF signal power observed. The different structure, especially the latent heat release profiles, associated with these two precipitation types may be of utility in better understanding the mechanism which produces the signal suppression observed.

In general most studies separate precipitation into stratiform or convective types (Houze, 1981, 1997; Drummond et al., 1996). Stratiform and convective precipitation can de defined in terms of their vertical velocity scales (Houze, 1997). Stratiform precipitation is defined as a precipitation process in which the vertical air motion is small compared to the fall velocity of ice crystals and snow. Ice crystals in the upper levels of the cloud play an important role in the precipitation process since precipitation particles that fall to the ground as raindrops have their early history as ice particles at upper levels. The low vertical velocities in stratiform precipitation allow the ice particles to grow via deposition, the time available for growth from cloud top being of the order of 1–3 h. Stratiform precipitation is fairly homogeneous in the horizontal giving it a layered structure in the vertical. In particular there is often a layer of pronounced Rayleigh Scatter enhancement, known as the bright band, associated with the melting layer (Doviak and Zrnić, 1993; Houze, 1997).

The convective precipitation process as defined in Houze (1997) differs sharply from stratiform precipitation and this is associated with the large vertical velocities in convection which equal or exceed the fall speeds of ice crystals and snow. The time available for the growth of precipitation particles is limited, being of the order of half an hour. This time is so short that precipitation particles must originate and grow not far above the cloud base. It is possible for growth to occur at this time because the updrafts are large enough to carry the growing particles upward until they become too heavy. Since the strong convective updrafts carrying the particles upward during the growth phase of the cloud condense large amounts of liquid water, the larger particles (which will move downward because of their larger terminal velocities) can grow readily by sweeping out the cloud water in their fall paths. For water drops, this process is called "coalescence" and in the case of ice particles it is known as "riming", these being the only microphysical growth mechanism rapid enough to explain the observations. From this viewpoint the magnitude of turbulent mixing within the cloud is important for these growth processes. Stratiform radar echoes contrast with convective precipitation which appears as cells (or horizontally localized patches). In vertical cross section, a cell is a tall, thin column of high reflectivity.

These different precipitation types display distinctly different vertical profiles of latent heat release to the atmosphere (Houze, 1997). The updrafts of the overturning cell (in convective precipitation) must transport more mass than the downdrafts for the net flux of air needed to account for the condensation of water in the layer. Stratiform regions are dominated by weaker air motions and cloud liquid water production is minimal. The convective mode therefore displays a heating release throughout the depth of the troposphere (associated with precipitation particles growing in the updraft), whereas the stratiform mode exhibits warming (from particle growth supported by rising air motion) in the region above the zero degree isotherm and a cooling (caused by melting and evaporation of particles in subsiding air) at levels below the zero degree isotherm.

It should be noted that not all studies have suggested that the clear-air return is suppressed during precipitation. For example, Cohn et al. (1995) made observations with a 915 MHz profiler in light precipitation and indicated that when rain or snow falls through a region of clear-air it modifies the humidity structure and possibly also influences the small-scale air circulation and thus may affect the returns. Their study focused on persistent clear air layers which can be examined before and during surface rainfall. The surprising feature of their study is that the clear air returns do not weaken, as might be expected if the humidity irregularities are smoothed out by evaporation, but actually strengthens. Their study can not explain this phenomena using thermodynamic affects because these would reduce the reflectivity of the clear air layer. Dynamical affects associated with the outer scale of turbulence are more difficult to predict. However, they do suggest that they observe no evidence for turbulent intensity increases and thus the enhanced UHF returns are not explained.

A brief description of each of the instruments used in this study and a short review of the measurement philosophy is detailed in Sect. 2. A technique to identify stratiform and convective precipitation using UHF UK Met Office wind profiler data is described in Sect. 3.1. The identification algorithm is then used in a statistical analysis aimed at identifying whether the characteristics of the signal suppression observed are different in differing precipitation regimes. Results of a statistical analysis are then detailed (Sect. 3.2). Finally, a case study of particular relevance to the questions raised by the statistical study is described in Sect. 3.3. Section 4 discusses possible interpretations of the observations detailed in Sect. 3.

2 Instruments and measurement strategy

The NERC MST radar at Aberystwyth (52.4° N, 4.1° W), described in Vaughan (2002), operates at a frequency of 46.5 MHz and has a peak transmitted power of 160 kW. The antenna consists of a 20 by 20 array of four element Yagi aerials covering an area of 110 m by 110 m. The radar beam has a one-way half-power half-width of 1.5 deg and it can be steered in sixteen possible directions. These include the vertical and at angles of 4.2, 6.0, 8.5 and 12.0 deg off-vertical in a variety of azimuths. However, in this study attention will be confined to the vertical beam observations only.

This radar derives parameters from Doppler spectra using a simple, single-peak spectral processing technique which has been developed for general purpose use rather than specifically for precipitation conditions. The mean noise power spectral density (PSD) is evaluated using the objective algorithm of Hildebrand and Sekhon (1974). The peak PSD within each spectrum is initially assumed to relate to the desired clear air radar return (subsequent reliability flagging, based on the time continuity of the Doppler shifts, is found to be effective at removing those spectra for which this assumption is clearly false). The spectral limits of the signal are bound by those points at which the PSD, to either side of the peak PSD, first drops below the mean noise PSD. For strong signals, the limits are further restricted by identifying those points at which the PSD first drops to 0.01 of the peak PSD. The principal spectral parameters of signal power, Doppler shift and spectral width are then calculated within these limits by the standard method described by Woodman (1985). Problems can arise when hydrometeor returns and clear air returns both contribute to the observed radar return signals. It is only under conditions of very heavy precipitation that the two components, observed by this radar, are distinct (Hooper et al., 2005). It is more common for the components to overlap, if a precipitation signal is observed at all, so that both are identified as belonging to a single signal (McDonald et al., 2004). In this situation the signal power will be overestimated and the spectral width may not be interpreted in terms of turbulence intensity without further analysis (Chu and Lin, 1994). It should be noted that more complicated processing schemes can be used to attempt to separate the characteristics of any precipitation signal from the clear air signal (Sato et al., 1990). An algorithm similar to that used in Rajopadhyaya et al. (1994) is used in Sect. 3.3. However, because the aim of this paper is to demonstrate the reduction in clear air radar return power associated with precipitation, the shortcoming of using the simple signal processing scheme will only mask the magnitude of the effect in cases where the signal power associated with precipitation is appreciable. Note that examination of Fig. 2 in Sect. 3 suggests that the vast majority of signals are unaffected by precipitation at least in a statistical sense.

The surface rainfall rate used in this study is measured by an ARG100 raingauge. The amount of rain collected is measured by the well-proven tipping bucket method. A contact closure at each tip is recorded by a datalogger and the number of tips during a 10-min interval is recorded. Thus, the rain gauge measures the integrated rainfall for a given time interval. In addition use is made of data from a (UK) Met Office 915 MHz (UHF) boundary-layer wind-profiler which was co-located with the NERC MST radar between 17 November 1999 and 11 March 2002. The useful altitude coverage of the UHF profiler varies with the measurement mode utilized and atmospheric conditions. It generally only extends significantly above 2 km when precipitation is present. Although the cycle time for observations is of the order of a few minutes, the data available for use in this statistical study represents consensus averages over 30 min. A limited amount of higher time resolution data is also used in the case study described in Sect. 3.3.

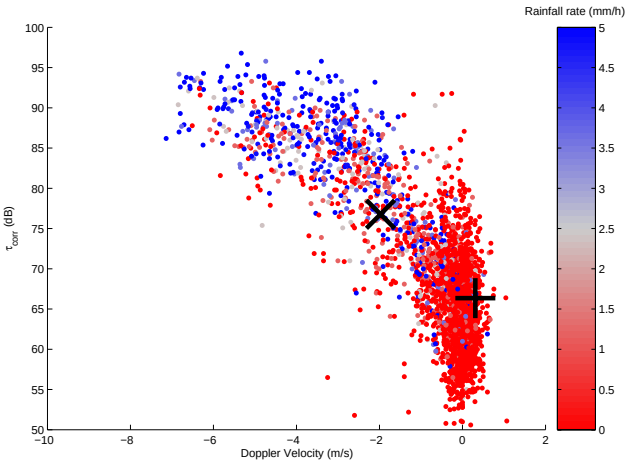

Fig. 1. Scatter plot of the variation of mean Doppler velocity and mean range squared corrected signal to noise ratio, τ_{corr}, obtained from the vertical beam of the UKMO UHF wind-profiler for the 68 days examined. Individual points are colour coded with the value of the surface rainfall rate measured by an ARG tipping bucket rain gauge. The centre of mass for the precipitation and no precipitation periods are identified by a plus sign and a cross, respectively.

3 Results

This study uses data from the NERC MST Radar facility at Aberystwyth in mid-Wales. An example of the effect of different types of precipitation on the observed signal power is shown after a statistical analysis of the effect of precipitation types on VHF returns. A total of 68 days between 31 August 2000 and 28 February 2002 inclusive were used in this study.

Figure 1 shows a scatter plot of the Doppler velocity against the range squared corrected signal to noise ratio observed by the vertical beam of the UK Met Office (UKMO) UHF wind profiler, the colour scale indicating the rainfall rate observed at the ground by a tipping bucket rain gauge. It should be noted that range squared corrected signal to noise ratios, τ_{corr}, have been used because this quantity is directly proportional to the reflectivity factor used more commonly by weather radar (Doviak and Zrnić, 1993). In addition, the use of τ_{corr} makes the determination of regions associated with a bright band and thereby stratiform precipitation amenable. Examination suggests that the UHF returns can be separated into two groups, the centre of mass of these two groups being displayed on the diagram. The first group associated with no surface rainfall covers a region associated with τ_{corr} values between 50 and 75 dB and Doppler velocities between –1 and 1 ms^{-1}. The Doppler velocities in this case are associated with the vertical component of the motion of the atmosphere because the returned signal is associated with clear air returns. The second group covers a much

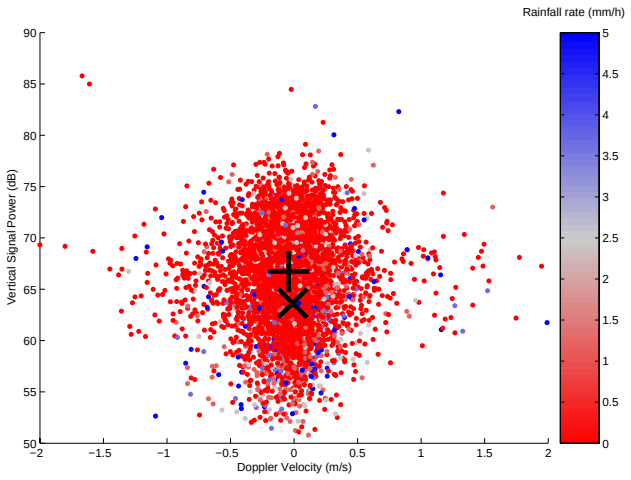

Fig. 2. Scatter plot of the variation of mean Doppler velocity and mean vertical signal power obtained using the VHF radar for the 68 days examined. Individual points are colour coded with the value of the surface rainfall rate measured by an ARG tipping bucket rain gauge. The centre of mass for the precipitation and no precipitation periods are identified by a plus sign and a cross, respectively.

wider range of Doppler velocities between 0 and –7 ms^{-1} (all downward) and τ_{corr} values between 75 and 95 dB and is associated with periods of precipitation. The second grouping results from enhanced returns associated with Rayleigh scattering from hydrometeors at this wavelength. Therefore the Doppler velocities in this case are associated with the net effect of the terminal fall speed of the hydrometeors and the air motion.

Figure 2 displays a scatter plot of the Doppler velocity against the signal power in the vertical beam observed by the NERC MST radar, the data points are colour coded to represent periods with different rainfall rates. Two groupings based on rainfall rates can be formed, the centre of mass of these two groups being displayed on the diagram. The first group associated with no surface rainfall covers a region associated with signal powers between 60 and 80 dB and Doppler velocities between –1 and 1 ms^{-1}. The second group covers a very similar range of Doppler velocities, but the range of signal powers varies between 50 and 70 dB and is associated with periods of precipitation. The fact that the averaged Doppler velocities in the data are similar during periods inside and outside precipitation suggests that the Doppler velocities during rainfall are largely unaffected by the returns from hydrometeors which will travel at a vertical velocity determined by the summation of their terminal velocity and the air's vertical velocity. The reduction in the observed vertical signal power during periods of rainfall also suggests that any enhancement associated with Rayleigh scatter is not, in general, significant at VHF wavelengths.

3.1 Stratiform and convective precipitation identification algorithm development and validation

A number of radar studies have indicated methods to distinguish stratiform and convective precipitation; most of these are dependent in some form on examining the reflectivity profile (or equivalent) for the presence of a bright band or other features (Bandera et al., 1998; Klassen, 1988; Williams et al., 1995). The majority of these studies have been used in conjunction with radar operating at microwave frequencies, the exception being Williams et al. (1995). Their study uses a combination of range squared corrected signal to noise ratio (which they call equivalent reflectivity), vertical velocity and spectral width to identify different rainfall types. Unfortunately, the time averaging of 30 min available for data in the majority of cases from the UKMO UHF profiler and the sparsity of reliable vertical velocity and spectral width data means that this study is limited to using profiles of the range squared corrected signal to noise ratio observed by the profiler's vertically orientated beam only.

Houze (1997) indicates that the presence of a bright band gives an unambiguous indicator of stratiform rain. However, the absence of a bright band does not guarantee the absence of stratiform rain. A strong bright band only occurs if some of the particles are in the form of large melting aggregates. Thus, a bright band indicates a certain type of stratiform precipitation. Thus, an algorithm to detect a bright band signature makes up the main component of the stratiform precipitation identification algorithm. In a similar manner to that used by Williams et al. (1995) regions associated with convective rainfall have been defined by identifying regions of enhanced range squared corrected signal to noise ratio that do not display a bright band structure and that are relatively uniform until a region above the melting layer.

A simple algorithm to identify bright bands has been developed, using similar methodologies to those discussed in Tilford et al. (1993) and Bandera et al. (1998). This algorithm uses the range squared corrected signal to noise ratio profile observed by the UHF radar to identify a bright band. It should be noted that previous to being passed to the algorithm this profile is passed through a three point running mean in altitude. The algorithm identifies the centre (or peak) of the bright band by examining the first and second derivative of the aforementioned profile. The minimum gradient marks the mid-point of the bright band lower limb and the maximum gradient marks the mid-point of the bright band upper limb. A further test uses the second derivative to ensure a maximum is observed. A bright band is then successfully identified when the feature identified has a peak greater than 85 dB, this value being specific to the wind-profiler, and a width no greater than 2.5 km. It should be noted that the UK Met Office UHF profiler transmits 1.4 μs pulses and thus has a range resolution of 200 m. This together with the three-point running mean and the fact that the 30-min consensus average acts to filter the data means that the width of the bright band can be over-estimated and thus only the position of the peak of the bright band is used in this study.

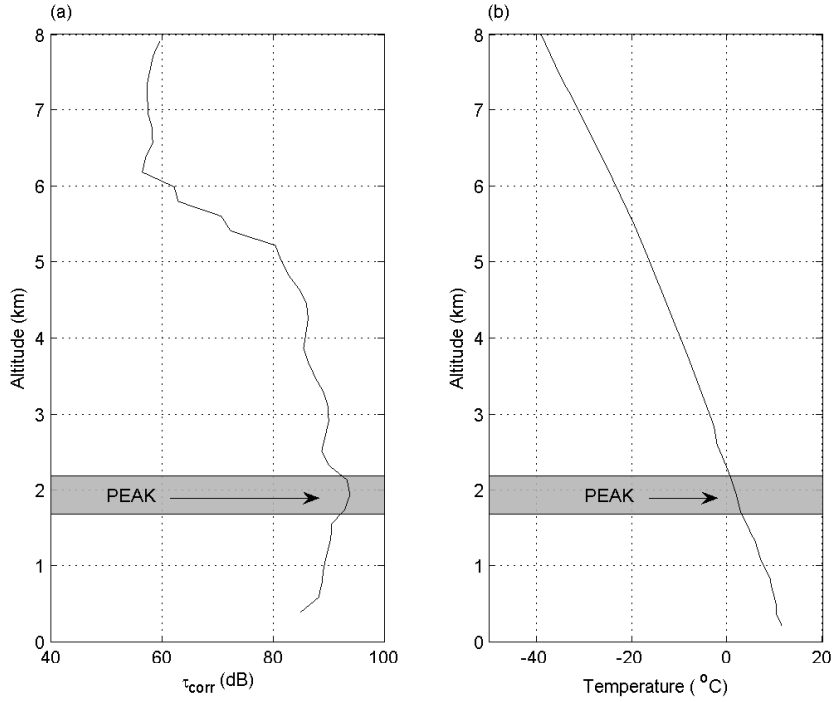

Fig. 3. Typical profiles of **(a)** range squared corrected signal to noise ratio, τ_{corr}, observed by the UKMO UHF wind profiler at Aberystwyth and **(b)** a near simultaneous radiosonde temperature profile launched from Aberporth (approximately 50 km away from the radar site) are displayed for the 11 December 2000 at 05:30 UT. The position of the peak of the bright band identified by the automated algorithm is also displayed.

A typical example of a UHF range squared corrected signal to noise ratio (τ_{corr}) profile associated with stratiform precipitation is displayed in Fig. 3a. A clear enhancement in τ_{corr} is observed with a peak at around 2 km. Figure 3a also shows the altitude of the centre of the bright band using the algorithm. Figure 3b displays a temperature profile measured by a radiosonde launched simultaneously from Aberporth, approximately 50 km from the radar site. Examination of the two profiles suggests that the peak of the bright band derived using the algorithm is approximately 400 m below the position of the zero degree isotherm observed in the temperature profile. The algorithm thus correctly identifies a period of enhancement associated with the melting layer and approximately the correct altitude. These facts are of prime importance in this study and a small error in the position of the bright band is acceptable.

By using surface rainfall data it is also possible to examine statistically whether this algorithm is identifying bright bands correctly. Using 3243 UHF profiles, a total of 970 profiles were associated with periods of surface rainfall, the algorithm identified a total of only 174 bright band features. Note that a bright band may not be observable during the early periods of rainfall and will not generally be observable during periods of convective rainfall. Table 1 displays a contingency table. The tetrachroic correlation for this contingency table is 0.76 (Brooks and Carruthers, 1953). Thus, surface rainfall and periods associated with a detected bright band are strongly correlated as should be expected.

Table 1. Contingency table which identifies the number of events associated with surface rainfall, observed using an ARG tipping bucket rain gauge, and the detection of a bright band (BB) signature identified in UHF UK Met Office wind-profiler data.

	No Rainfall	Rainfall
BB not detected	2231	796
BB detected	42	174

To further examine whether the bright band detection algorithm performs as expected temperature data from the UK Met Office mesocale version of the unified model (Cullen, 1993) has been utilized to determine whether the position of the bright band peak identified by the algorithm corresponds to a position below that of the zero degree isotherm. The data utilized covers the period 10 to 12 December 2000 and corresponds to a period when the bright band detection algorithm identified a total of 14 separate bright bands. Examination of Fig. 4 shows that the correspondence between the position of the zero degree isotherm and that of the peak of the bright band is generally excellent. The rapid change in the altitude of the zero degree isotherm at around 21:00 UT on 10 December 2000 and 18:00 UT on 12 December 2000 are associated with periods of frontal passage over Aberystwyth. Only two periods show the position of the bright

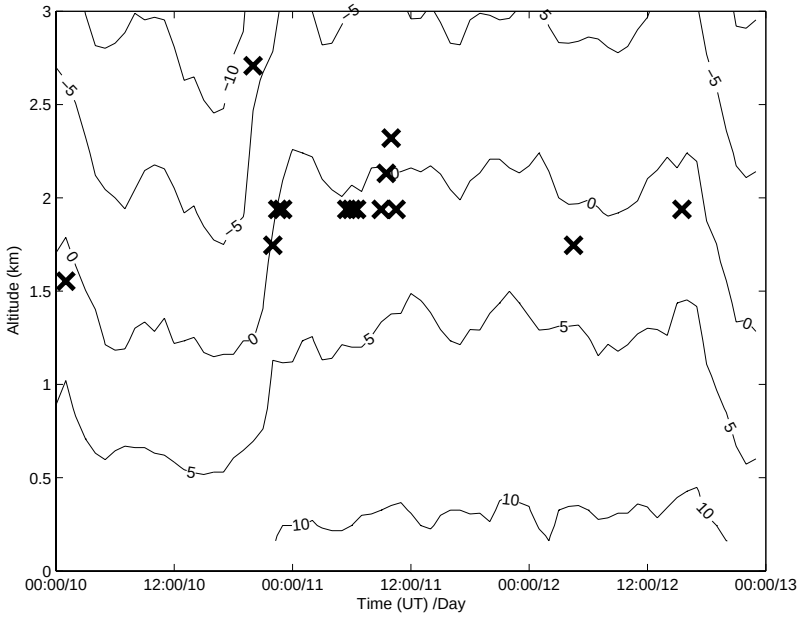

Fig. 4. Time-height contour plot of temperature taken from the UK Met Office mesoscale model predictions over Aberystwyth for the period 10 to 12 December 2000. Also displayed are crosses which indicate the position of the peak of the bright band identified by the bright band detection algorithm during this period.

Table 2. Contingency table which identifies the number of events associated with surface rainfall, observed using an ARG tipping bucket rain gauge, and the detection of a convective signature identified in UHF UK Met Office wind-profiler data.

	No Rainfall	Rainfall
convection not detected	2264	914
convection detected	9	56

band being significantly greater than that of the zero degree isotherm these occur at 20:00 UT on the 10 December 2000 and on 10:00 UT on the 11 December 2000. Comparison of the mesoscale model data with radiosonde data, radiosonde measurements from the close by Aberporth site (see Fig. 3b) were available from launches at 06:00 and 16:00 UT on the 11 December and 05:00 UT on the 12 December 2000, indicate that the second of these points may be real since the position of the zero degree isotherm in the radiosonde data is roughly 200 m higher than that in the model at the same time. However, the first point seems anomalous and is suggested to be associated with a cloud top which Tilford et al. (1993) indicates is sometimes a problem. However, the results displayed in Figs. 3 and 4 and also Table 1 indicate that the bright band identification algorithm works effectively in the vast majority of cases.

As previously indicated the convective precipitation identification algorithm identifies profiles that do not display a bright band structure and that are relatively uniform until above the melting layer. It was found that a mean value of τ_{corr} of 80 dB in the first 5 km of the atmosphere and a period without a bright band signature produces a reasonable identification of convective precipitation periods for the particular UHF data under consideration. Table 2 displays a contingency table, which allows the correspondence between convective periods identified by the algorithm and periods of surface rainfall measured by an ARG tipping bucket rain gauge to be examined. The tetrachroic correlation for this contingency table is 0.8. Thus, surface rainfall and periods associated with a detected convective rainfall period are strongly correlated as should be expected. Examination of the contingency table suggests that of the 3243 UHF profiles the algorithm identified a total of only 65 convective features which represents a total of 32.5 h of observations. It should be noted that Houze (1997) indicates that, at least in the tropics, it is difficult to identify a large portion of the rainfall as either convective or stratiform and therefore the large number of surface rainfall periods not clearly identified as either precipitation type should perhaps be expected.

3.2 Statistical analysis

It was previously indicated in McDonald et al. (2004), using 33 days of data from 2001 that the mean VHF signal power decreases during periods of rainfall. It was also observed that the spectral width increases during periods of rainfall. However, the small number of observations made it impossible to separate the rainfall into different types. In this study a statistical analysis showing the relation between stratiform and convective precipitation, identified using the techniques indicated in Sect. 3.1, and VHF radar signal suppression is examined. This study uses a total of 68 days between 31 August

Table 3. The mean VHF signal power averaged over the height range indicated during periods where the indicated rainfall threshold was and was not exceeded is shown. In addition the number of positive and negative changes in the mean signal power associated with rainfall and the number of significant decreases in the signal power associated with periods of surface rainfall above the indicated threshold are shown. The surface rainfall is observed by a tipping bucket rain gauge co-located with the VHF radar.

Height range (km)	Mean VHF signal power during periods when the surface rainfall threshold was exceeded (dB)	Mean VHF signal power during periods when the surface rainfall threshold was NOT exceeded (dB)	Values (increase/decrease)	Significant decreases/Total
2–4	63.5	65.4	20/48	32/68
4–6	56.0	56.0	34/34	16/68

Table 4. The mean VHF signal power averaged over the height range indicated during periods where a Bright band was detected by the automated algorithm described in Sect. 3.1. In addition the number of positive and negative changes in the mean signal power associated with the presence of a bright band and the number of significant decreases in the signal power associated with periods which displayed the presence of a bright band are displayed.

Height range (km)	Mean VHF signal power during period when stratiform rain was identified	Mean VHF signal power during periods when the stratiform rain was NOT observed	Values (increase/decrease)	Significant decreases/Total
2–4	61.6	65.2	5/44	25/49
4–6	54.6	55.8	18/31	10/49

2000 and 28 February 2002 inclusive to increase the number of observations used in the previous study.

Table 3 shows the mean signal power, for two altitude regions, associated with periods with and without surface precipitation. When the mean signal power is calculated from VHF data between 2 and 4 km using a rainfall threshold of $0\,\mathrm{mm\,h^{-1}}$ (rain and no rain periods) a decrease of 1.9 dB is observed during rainfall. Between 4 and 6 km no difference is observed. Table 3 also displays the number of days in which significant differences at the 95% confidence level are observed for the two categories, these categories being surface rainfall and no surface rainfall. Examination suggests that VHF signal power reductions are observed just under half of the time. The values displayed in Table 3 are broadly consistent with the previous results discussed in McDonald et al. (2004).

Table 4, similarly to Table 3, displays the mean signal power for two altitude regions. However, in this case the data is separated into regions identified as stratiform precipitation periods and periods without surface rainfall. Examination suggests that for VHF signal powers averaged between 2 and 4 km have a value of 61.6 dB during periods associated with a bright band and outside the surface rainfall period have an average value of 65.2 dB. The signal power decrease for stratiform precipitation is a factor of two larger than that observed under all rainfall conditions (c.f. Table 3 and Table 4). This suggests that the particular type of stratiform precipitation identified by the algorithm suppresses the VHF signal more efficiently than all rainfall types. Examination of the frequency of occurrence of significant differences displays a very small change in percentage terms compared to periods associated with all rainfall types, these values being 47 and 51%, respectively. Thus, it seems likely that stratiform rainfall may have a larger impact on the VHF signal than other types of rainfall. But, that the observed VHF signal reductions are not specific to processes occurring in stratiform precipitation. It should be noted that only 49 days were used out of the possible 68 days, this was because only 49 days displayed stratiform precipitation with periods greater than or equal to 1 h and were thus of use in the statistical analysis.

Data utilizing VHF signal power averages derived between 4 and 6 km (shown in Table 4) suggest that the strength of the VHF signal suppression observed is smaller than that at lower altitudes. This difference might be associated with the position of the observations relative to the bright band because stratiform precipitation exhibits warming (from particle growth supported by rising air motion) in the region above the zero degree isotherm and a cooling (caused by melting and evaporation of particles in subsiding air) at levels below the zero degree isotherm. The possibility of the suppression phenomena being related to evaporation could perhaps explain this observation. However, examination of the average altitude of bright bands suggests that it is more likely that this observation is purely related to the maximum vertical extent of the precipitating clouds.

Table 5. The mean VHF signal power averaged over the height range indicated during periods where convective precipitation was and was not detected are shown. In addition the number of positive and negative changes in the mean signal power associated with convective precipitation and the number of significant decreases in the signal power associated with periods of convective precipitation are shown.

Height range (km)	Mean VHF signal power during periods when convective rain was observed	Mean VHF signal power during periods when convective rain was NOT observed	Values (increase/decrease)	Significant decreases/Total
2–4	61.8	65.2	0/15	4/15
4–6	55.7	56.3	8/7	2/15

Table 5 represents the mean signal power for two altitude regions separated into periods inside and outside convective precipitation detected in the UHF range squared corrected signal to noise ratio. Examination suggests that for VHF signal powers averaged between 2 and 4 km periods which display convective precipitation characteristics have an average value of 61.8 dB and periods in which a convective signature was not identified have an average signal power of 65.2 dB. These values collate well with those during stratiform precipitation, identified by the presence of a bright band. This again is a factor of two greater than that derived under all rainfall conditions defined by the tipping bucket surface rain gauge. This suggests that the identification algorithms, for both stratiform and convective precipitation, may be identifying only the clearest precipitation periods. However, the frequency of occurrence of significant differences displays a much smaller value than that during other rainfall periods, that being 27 and 47%, respectively.

Table 5 also represents the mean signal power for data between 4 and 6 km. Examination in this case suggests that the mean VHF signal power is again reduced during and outside periods of convective precipitation, the values being 55.7 and 56.3 dB, respectively. It should be noted that only 15 days were used in this statistical analysis out of the possible 68 days, this was because only 15 days displayed convective precipitation with periods greater than or equal to one hour and were thus of use in the statistical analysis. It should be noted that the statistics presented in Table 3 to 5 change very little if only data that has a clear stratiform or convective signal and also correspond to periods of surface precipitation are accepted. It was also found that varying the thresholds used in the stratiform and convective precipitation algorithms had little effect on the statistics obtained.

It should also be noted that these results are consistent with previous work detailed in McDonald et al. (2004). The analysis discussed in McDonald et al. (2004) suggests that the position of the zero degree isotherm relative to the region of signal suppression does not have a significant affect on the amount of suppression observed. This lack of impact compared with observations in the tropics (Chu et al., 1991) is suggested to be associated with the fact that the bright band has a very different structure at mid-latitudes.

3.3 Case study: 24 September 2000

In the previous section, it was shown that in stratiform precipitation VHF signal suppression is observed 51% of the time while in convective precipitation suppression is observed only 27% of the time at 2–4 km. Table 3 also suggests that this phenomenon occurs during all types of precipitation. Some process that is not as active in convective precipitation therefore seems necessary to explain these observations. As indicated previously the two mechanisms suggested to account for the observed VHF signal suppression are evaporation smoothing small-scale irregularities in the humidity profile and entrainment. Given the information discussed in Houze (1997) about the different latent heat release profiles observed for stratiform and convective precipitation it seems likely that evaporation may be the most important mechanism. This section examines a set of data obtained on 24 September 2000 which has some interesting features which are of use in determining the likelihood of the two mechanisms being important contributors to the VHF signal suppression mechanism.

Figure 5a displays a time height contour plot of the VHF signal power derived on the 24 September 2000 between 03:00 and 13:00 UT. Figures 5b and c display time height contour plots of the τ_{corr} and vertical velocity, respectively. It should be noted that high time resolution UHF data was available on this date. The resolution of this data being approximately 2 min rather than the half hour consensus averages used previously in the statistical study described in Sect. 3.2. Comparison of the vertical signal power from the VHF wind-profiler and τ_{corr} from the UHF profiler shown in Figs. 5a and b, respectively, indicates a number of similar features. The two most distinct features observed in the UHF wind-profiler data are periods of rainfall observed between approximately 03:30 and 04:00 UT between 2 and 4 km and the large cloud shaped structure between approximately 06:30 and 12:30 UT which extends from roughly 3 to 6 km. The first feature displays a clear enhancement in the UHF τ_{corr} (see Fig. 5b) and a region of large downward velocities (see Fig. 5c). These signatures are indicative of UHF signal enhancements associated with returns from Rayleigh scattering from hydrometeors moving with a vertical velocity which is a summation of the terminal velocity of the particles and the background wind velocity. It should be noted that the

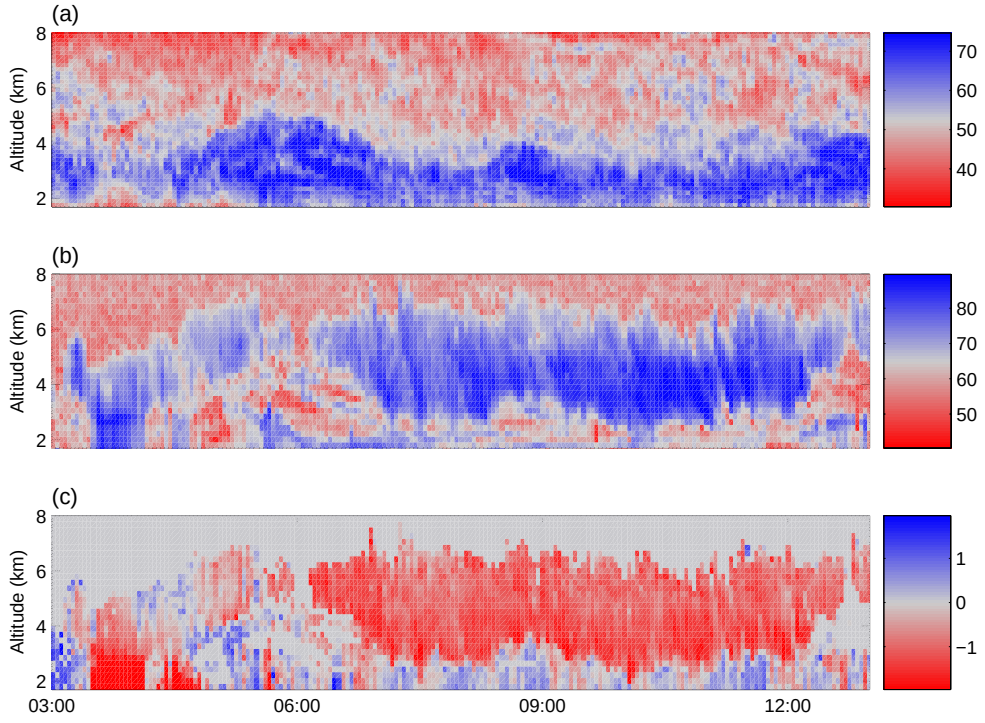

Fig. 5. Time-height contour plots of **(a)** vertical signal power (dB) observed by VHF radar, **(b)** the vertical range squared corrected signal to noise ratio (dB) and **(c)** the vertical velocity (ms^{-1}) measured by a co-located UHF wind profiler observed on 24 September 2000. Note that the UHF data has a higher time resolution than that available in the rest of this study.

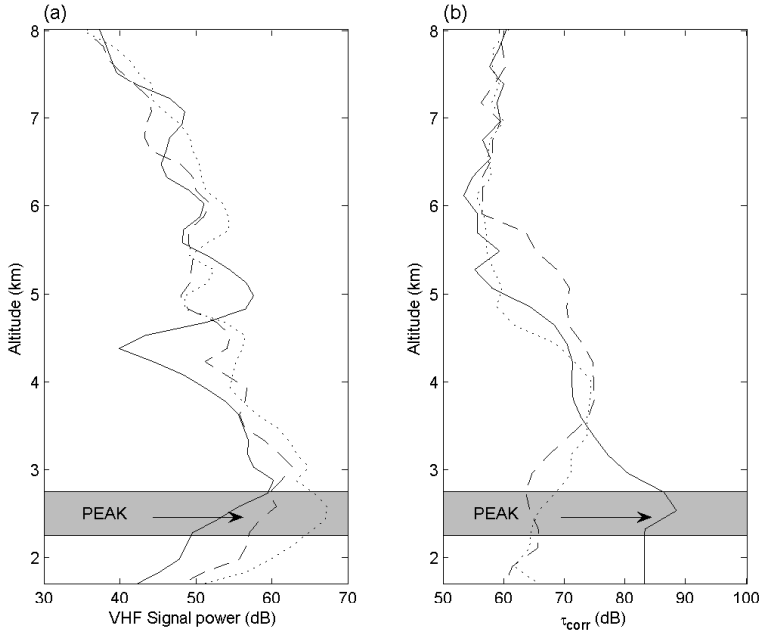

Fig. 6. Profiles of **(a)** vertical signal power (dB) observed by VHF radar and **(b)** the vertical range squared corrected signal to noise ratio (dB) measured by a co-located UHF wind profiler on 24 September 2000. The dotted line indicates the profile for 03:20 UT (outside a period of surface precipitation), the full line the profile for 03:45 UT (inside a period of surface precipitation) and the dashed line the profiles for 04:20 UT (outside a period of surface precipitation). Also displayed is a shaded region which indicates the position of the peak of the bright band identified by the Bright band detection algorithm during this period.

bright band identification algorithm also classifies this region as a period of stratiform precipitation. The peak of the bright band being identified at approximately 2.6 km.

Figure 6a displays the VHF signal power at three times before, during and after the stratiform precipitation. Examination of these profiles suggests that the VHF signal power profiles are relatively similar before and after the precipitation, but that at altitudes between 1.7 and 4 km the VHF signal power is reduced during stratiform precipitation. Examination of the range squared corrected signal to noise ratio profiles shown in Fig. 6b suggests that a bright band can be observed at approximately 2.6 km, this also being indicated by the bright band detection algorithm. Further examination of Fig. 6a also indicates that the minimum difference between inside and outside stratiform precipitation events occurs close to but slightly above the bright band enhancement. A similar feature is also observed in Rao et al. (1999) (see their Fig. 4). This observation suggests that the zero degree isotherm may have some modulating effect on the VHF signal suppression observed. But, it is noticeable that the difference between the profiles for data before and during stratiform precipitation periods are of near equal value above and below the bright band on average. This does not correspond well with the fact that in general stratiform precipitation exhibits warming (from particle growth supported by rising air motion) in the region above the zero degree isotherm and a cooling (caused by melting and evaporation of particles in subsiding air) at levels below the zero degree isotherm.

The second feature observed between 06:30 and 12:30 UT seems to be associated with a precipitating cloud. It should be noted at this point that this cloud displays a number of characteristics, altitude and form of the cloud, which indicate it is likely to have a high ice water content. The boundaries of this cloud structure have been identified by finding those regions which have τ_{corr} values above 75 dB and downward vertical velocities in the UK Met Office UHF wind-profiler data and these cloud boundaries are superimposed on the VHF data shown in Fig. 7. Examination of the range squared corrected signal to noise ratio profile does not show evidence of a bright band in this case and this is probably associated with the fact that the precipitation seems to have completely evaporated at around 3 km slightly above the altitude of the melting level. No other explanation for the disappearance of the precipitation at this level seems likely in our view and this identification of a region associated with active evaporation and its importance is discussed later in this section.

Figure 7 displays time height contour plots of the vertical spectral width (corrected for beam-broadening), and the signal power perturbation between 06:00 and 13:00 UT on 24 September 2000. The signal power perturbation has been calculated by removing the mean signal power profile, derived using the mean for signal powers before and after the cloud, from the VHF signal power. Comparison of the spectral width derived by the VHF radar and the cloud boundary, both shown in Fig. 7a, suggests that enhanced spectral widths are observed preferentially close to or below the cloud base. It should be noted that spectral width enhancements are generally associated with regions of turbulence. However, the interpretation of enhanced spectral widths observed by VHF profilers is generally more difficult during periods of precipitation (Chu and Lin, 1994).

To determine the origin of the enhanced spectral widths observed near the cloud base a more complicated signal processing scheme similar to that described in Rajopadhyaya et al. (1994) has been used. This algorithm selects two peaks in Doppler spectra in which both precipitation and clear-air signals can be identified in a statistical manner. Figures 8a and b display the spectral width associated with the precipitation and the clear-air signals, respectively, a threshold value has been used on the precipitation signals so that only relatively large precipitation signals capable of contributing to the combined signal significantly are displayed in Fig. 8b. Figure 8c shows the vertical velocities associated with the clear-air component of the returns. Examination of Fig. 8c suggests no preferential direction of motion for these signals in the vertical direction, the values of the vertical velocities for the precipitation signal (not shown) on other hand are always downward. This suggests that the algorithm works well at identifying and separating the precipitation and clear-air signals in general. Examination of the spectral widths in Fig. 8a suggests that precipitation signals are preferentially observed in the region of enhanced spectral widths previously displayed in Fig. 7a. However, the values of the spectral widths associated with the clear-air component of this signal are still enhanced in this region even after the contribution from the precipitation signal has been corrected (see Fig. 8b). It should be noted that the spectral widths displayed in Fig. 8 are significantly larger than those identified in Fig. 7 because no attempt has been made to correct for beam broadening in this case. Thus, it seems that hydrometeor contamination only accounts for some of the enhanced spectral width. It should be noted that when the precipitation and clear-air signals are strongly overlapped it is sometimes very difficult to separate these signals and thus hydrometeor contamination could feasibly explain all of the enhanced spectral width observed in Fig. 7a.

While there is a possibility of hydrometeor contamination producing the enhanced spectral widths observed, previous work by Bouniol et al. (2004) using cloud radar has observed similar structure in calculated values of the turbulent kinetic energy dissipation rate. Work described in Albrecht and Kollias (2001) also suggests that in-cloud turbulence is preferentially observed at cloud base. In addition the fact that the enhanced spectral width region follows so closely the precipitating cloud base suggests that in this case the enhancements are associated with turbulence. Bouniol et al. (2004) suggests that large values of turbulent kinetic energy dissipation rates at cloud base can be explained by evaporation of ice particles falling in an unsaturated environment, this evaporation absorbs latent heat which tends to increase the mixing processes. This region of entrainment is of particular relevance because it suggests that if entrainment plays a role in the VHF signal suppression then the suppression should be particularly strong close to these altitudes.

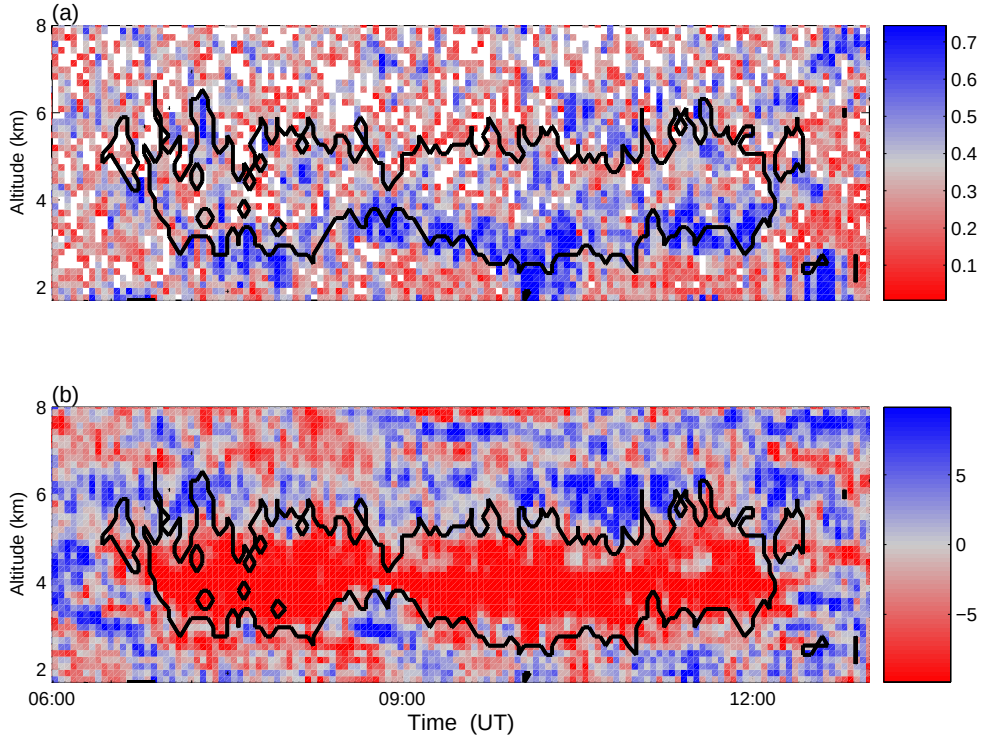

Fig. 7. Profiles of **(a)** vertical spectral width (ms^{-1}) and **(b)** vertical signal power perturbation (dB) observed by the VHF wind profiler on 24 September 2000. The full line indicates the extent of precipitating cloud regions identified using simultaneous UHF wind profiler data.

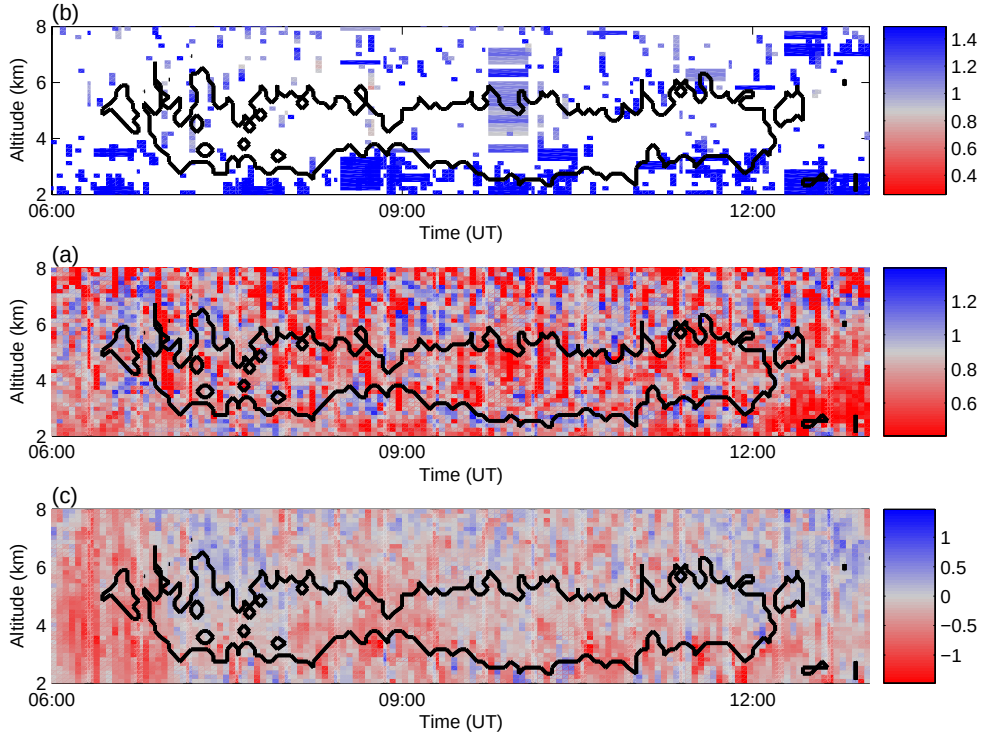

Fig. 8. Profiles of **(a)** precipitation signal spectral width (ms^{-1}), **(b)** clear-air signal spectral width (ms^{-1}), and(c) clear-air vertical velocity (ms^{-1}) observed by the VHF wind profiler on 24 September 2000. The full line indicates the extent of precipitating cloud regions identified using simultaneous UHF wind profiler data.

Figure 7b displays a time height contour plot of the signal power perturbation. Positive (negative) values of the signal power perturbation relate to regions where the VHF signal power is enhanced (suppressed) relative to the mean VHF signal power profile calculated using the mean of signal powers before and after the cloud is observed. Examination of Fig. 7b shows no particular structure outside the cloud boundaries with nearly equal areas of VHF signal power enhancement and suppression being observed. In stark contrast the VHF signal power is observed to only be suppressed in the interior of the cloud defined by the boundary. It should also be noted that the VHF signal suppression seems to be relatively uniform throughout the cloud region. This correspondence is excellent given the totally independent nature of the cloud boundary derived using UHF wind profiler data and the VHF radar data. The correspondence is so good that the narrowing of the clouds vertical extent observed just before 09:00 UT is also observed in the VHF signal power perturbation for instance. In fact this correspondence is so good that it suggests that this technique may have utility in allowing cloud structure to be identified by VHF wind profilers routinely.

It should be noted that the boundaries of the cloud structure relate to the region of precipitation and may not relate to the cloud top or cloud base. However, information previously described in this section and discussed in Bouniol et al. (2004) and Albrecht and Kollias (2001) leads us to the conclusion that these boundaries also define the cloud base and cloud top accurately in this case. The clear region of evaporation identified at cloud base is of particular relevance because it suggests that the region above this level is saturated. It is possible that this saturated region is produced by the evaporation of precipitation some time previous to the observation. This possibility also corresponds well with the data in Fig. 7b which could show regions of strong suppression where evaporation has already occurred. The evaporation at the bottom of the cloud would then therefore be an unsaturated region (this may become saturated later) which would be related to only partial signal suppression. This interpretation would suggest that if evaporation plays a role in the VHF signal suppression then the suppression should be particularly strong above the evaporation region and less strong in this region. Thus, it seems likely that identification of regions of strong signal suppression could be of use in identifying the relative importance of the two mechanisms previously indicated.

Another possibility that could partially explain the fact that the signal suppression is observed only in the interior of the cloud is associated with the fact that the cloud may be associated with a high ice water content. This change could therefore change the saturation water vapor pressure because this quantity has a different value on the surface of liquid water from that on the surface of solid ice particles. However, evidence for a high ice water content in the cloud is only circumstantial.

4 Discussion and conclusions

The development of automated algorithms to define periods associated with stratiform and convective precipitation using UHF range squared corrected signal to noise ratio profiles has been described and demonstrated to be efficient. Separation of precipitation periods into stratiform and convective regions is performed to examine the affect of these precipitation types on the VHF signal power return. Statistical analysis suggests that both precipitation types produce similar magnitude reductions in VHF signal power on average. However, the frequency of occurrence of statistically significant reductions in VHF signal power are very different. At 2–4 km stratiform precipitation shows VHF signal suppression is observed 51% of the time while in convective precipitation suppression is observed only 27% of the time. Using the subset of days which contains both stratiform and convective precipitation increases the stratiform value to 53% and leaves the convection value unchanged. Given the information discussed in Houze (1997) this suggests that evaporation may be an important mechanism in explaining the observed VHF signal suppression. It should be noted that the observed similarity in the VHF signal power response for convective and stratiform precipitation is supported by previous analysis in McDonald et al. (2004). Their analysis indicates that little variation in the VHF signal suppression is observed as a function of rainfall rate. Given that convective precipitation is normally associated with significantly higher rainfall rates than those related to stratiform precipitation their result suggests a similar conclusion to that identified in the current work.

The case study discussed in Sect. 3.3 examines an event where both regions of evaporation and also possibly turbulent entrainment can be identified. As previously indicated, evaporation has been suggested to act to smooth out small-scale irregularities in humidity bringing the air towards the local saturated vapour pressure and thus producing a VHF signal suppression by removing the humidity component of the small-scale irregularities in the radio refractive index profile. The fact that the signal suppression observed in Fig. 7b is predominantly above the region of evaporation (i.e. in a saturated region) is in line with the hypothesis of evaporation removing small-scale irregularities in humidity. The reduction in the VHF suppression at the evaporation level also supports the idea that in the unsaturated region the evaporation of hydrometeors has not removed all the small-scale irregularities in the humidity profile. Thus, the detailed case study presented suggests that evaporation reducing small-scale irregularities could be important. The possibility of affects associated with changes in saturation vapour pressure can also not be ruled out.

Regions of enhanced spectral width are also observed and we believe these are associated with enhanced turbulence rather than over-estimations associated with precipitation and clear-air signals overlapping (Chu and Lin, 1994). The proximity of the enhanced spectral width region to the region identified as being associated with evaporation also

suggests that this measurement is associated with turbulence. In particular, the region of strong evaporation would act to release latent heat which tends to increase the mixing process. Given the lack of structure in the signal power perturbation (see Fig. 7b) near the turbulent region it seems that this mechanism may not be important in producing the observed VHF signal suppression. However, it should be noted that given the right conditions it might be possible for the effects of turbulent entrainment and evaporation to cancel out such that the signal suppression would not be enhanced in the region specified.

Acknowledgements. A. J. McDonald would like to acknowledge grant U6518 awarded by the University of Canterbury. The MST Radar Facility at Aberystwyth is funded by the UK Natural Environment Research Council and the data presented in this paper has been kindly provided through the British Atmospheric Data Centre. We would also like to thank the (UK) Met Office who kindly provided the Mesoscale model, UHF wind profiler and high resolution radiosonde data to this work through the British Atmospheric Data Centre.

Topical Editor F. D′Andréa thanks two referees for their help in evaluating this paper.

References

Albrecht, A. and Kollias, P.: Turbulence observations in layer clouds, in: 31st international conference on radar meterology, http://ams.confex.com/ams/32BC31R5C/techprogram/session_16003.htm, 2001.

Bandera, J., Papatsoris, A. D., Watson, P. A., Tan, J., and Goddard, J. W.: Method for detecting the extent of the melting layer, Electronics Letters, 34, 2104–2105, 1998.

Bouniol, D., Illingworth, A., and Hogan, R.: Deriving turbulent kinetic energy dissipation rate within clouds using ground based radar, in: ERAD 2004, 281–285, 2004.

Brooks, C. E. P. and Carruthers, N.: Handbook of statistical methods in meteorology, HMSO, London, 1st edn., 1953.

Chu, Y.-H. and Lin, C.-H.: The severe depletion of turbulent echo power in precipitation observed using the Chung-Li VHF Doppler radar, Radio Science, 29, 1311–1320, 1994.

Chu, Y. H. and Song, J.-S.: Observations of precipitation associated with a cold front using a VHF wind profiler and a ground-based optical rain gauge, J. Geophys. Res., 103, 11 401–11 409, 1998.

Chu, Y. H., Chian, L. P., and Liu, C. H.: The investigation of the atmospheric precipitations by using Chung-Li VHF radar, Radio Science, 26, 717–729, 1991.

Cohn, S. A., Rogers, R. R., Jascourt, S., Ecklund, W. L., Carter, D. A., and Wilson, J. S.: Interactions between Clear-Air Reflective Layers and Rain Observed with a Boundary-Layer Wind Profiler, Radio Science, 30, 323–341, 1995.

Cullen, M. J. P.: The Unified Forecast/Climate Model, Meteorological Magazine, 122, 81–94, 1993.

Doviak, R. J. and Zrnić, D. S.: Doppler Radar and Weather Observations, Academic Press, San Diego, 2nd edn., 1993.

Drummond, F. J., Rogers, R. R., Cohn, S. A., Ecklund, W. L., Carter, D. A., and Wilson, J. S.: A new look at the melting layer, J. Atmos. Sci., 53, 759–769, 1996.

Hildebrand, P. H. and Sekhon, R. S.: Objective determination of the noise level in Doppler spectra, J. Appl. Met., 13, 808–811, 1974.

Hooper, D. A., McDonald, A. J., Pavelin, E., Carey-Smith, T. K., and Pascoe, C. L.: The signature of mid-latitude convection observed by VHF wind-profiling radar, Geophys. Res. Lett., 32, 2005.

Houze, R. A.: Structures of Atmospheric Precipitation Systems – a Global Survey, Radio Science, 16, 671–689, 1981.

Houze, R. A.: Stratiform precipitation in regions of convection: A meteorological paradox?, Bulletin of the American Meteorological Society, 78, 2179–2196, 1997.

Klassen, W.: Radar observations and simulation of the melting layer of precipitation, J. Atmos. Sci., 45, 3741 –3753, 1988.

McDonald, A. J., Carey-Smith, T. K., Hooper, D. A., Fraser, G. J., and Lublow, B. P.: The effect of precipitation on wind-profiler clear air returns, Ann. Geophys., 22, 3959–3970, 2004, **SRef-ID: 1432-0576/ag/2004-22-3959**.

Rajopadhyaya, D. K., May, P. T., and Vincent, R. A.: The retrieval of ice particle size information from VHF wind profiler Doppler spectra, J. Atmosp. Oc., 11, 1559–1568, 1994.

Ralph, F. M.: Using radar-measured radila vertical velocities to distinguish Precipitation scattering from Clear-air scattering, J. Atmosp. Oc., 12, 257–267, 1995.

Rao, T., Rao, D., and Raghavan, S.: Tropical precipitating systems observed with Indian MST radar, Radio Science, 34, 1125–1139, 1999.

Sato, T., Doji, H., Iwai, H., Kimura, I., Fukao, S., Yamamoto, M., Tsuda, T., and Kato, S.: Computer-processing for deriving drop-size distributions and vertical air velocities from VHF Doppler radar spectra, Radio Science, 25, 961–973, 1990.

Tilford, K. A., Han, D., and Cluckie, I. D.: Vertically Pointing and Urban Weather radars, Academic Press, San Diego, 2nd edn., 1993.

Vaughan, G.: The UK MST radar, Weather, 57, 69–73, 2002.

Vaughan, G. and Worthington, R. M.: Effects of humidity and precipitation on VHF radar vertical beam echoes, Radio Science, 35, 1389–1398, 2000.

Williams, C. R., Ecklund, W. L., and Gage, K. S.: Classification of Precipitating clouds in the Tropics using 915 MHz Wind Profilers, J. Atmosp. Oc., 12, 996–1012, 1995.

Woodman, R. F.: Spectral moment estimation in MST radars, Radio Science, 20, 1185–1195, 1985.